Dynamic prediction modelling and equilibrium stability of a fractional discrete biophysical neuron model

Maysaa Al-Qurashi [a,b,1], Saima Rashid [c,*,1], Fahd Jarad [d,e,*,1], Elsiddeg Ali [f,1], Ria H. Egami [g,1]

[a] Department of Mathematics, King Saud University, P.O. Box 22452, Riyadh 11495, Saudi Arabia
[b] Department of Mathematics, Saudi Electronic University, Riyadh, Saudi Arabia
[c] Department of Mathematics, Government College University, Faisalabad 38000, Pakistan
[d] Department of Mathematics, Faculty of Arts and Science, Çankaya University, Ankara, 06790, Turkey
[e] Department of Medical Research, China Medical University, Taichung 40402, Taiwan
[f] Department of Mathematics, Turabah University College, Taif University, P.O. Box 11099, Taif 21944, Saudi Arabia
[g] Department of Mathematics, College of Science and Humanities in Sulail, Prince Sattam Bin Abdulaziz University, Saudi Arabia

ARTICLE INFO

ABSTRACT

Here, we contemplate discrete-time fractional-order neural connectivity using the discrete nabla operator. Taking into account significant advances in the analysis of discrete fractional calculus, as well as the assertion that the complexities of discrete-time neural networks in fractional-order contexts have not yet been adequately reported. Considering a dynamic fast–slow FitzHugh–Rinzel (FHR) framework for elliptic eruptions with a fixed number of features and a consistent power flow to identify such behavioural traits. In an attempt to determine the effect of a biological neuron, the extension of this integer-order framework offers a variety of neurogenesis reactions (frequent spiking, swift diluting, erupting, blended vibrations, etc.). It is still unclear exactly how much the fractional-order complexities may alter the fring attributes of excitatory structures. We investigate how the implosion of the integer-order reaction varies with perturbation, with predictability and bifurcation interpretation dependent on the fractional-order $\beta \in (0, 1]$. The memory kernel of the fractional-order interactions is responsible for this. Despite the fact that an initial impulse delay is present, the fractional-order FHR framework has a lower fring incidence than the integer-order approximation. We also look at the responses of associated FHR receptors that synchronize at distinctive fractional orders and have weak interfacial expertise. This fractional-order structure can be formed to exhibit a variety of neurocomputational functionalities, thanks to its intriguing transient properties, which strengthen the responsive neurogenesis structures.

Introduction

The fundamental building blocks of neural circuitry are neurons. Because of their interdependence, they can achieve gratification and excitement when collaborating together. It is thought that neurotransmitters play a crucial role in signal analysis. A nerve cell system's firing behaviour of neural connections, which seems characterized by the meditation perturbation method for generating and communicating nerve impulses, is how documentation is encrypted, transferred, and demodulated [1]. The primary mechanism of neurotransmission is explosion, which alternates between a dormant stage and a repeated stimulatory condition.

Significant nervous processes can exhibit numerous erupting structures. Numerous scholars have investigated the concussive structures seen in various artificial neural network in some instances, neuro-electroencephalographic researchers, epidemiological and biophysical scientists have indeed supported these findings [2–6]. The publications by Rinzel and his colleague, which presented three regularities (square-wave, parabolic and elliptic kinds of erupting) and whose structures of exploding were illustrated by the inter-spike time-frame property but were unrelated to the progression of the dynamic loading [7,8], are among the earliest examples regarding exploding categorization. Subsequently, the different forms mentioned above were given the designations Class I, II, and III, respectively, for characterization. A specific form, Class IV, which exhibits an anomalous inter-spike time-frame characteristic, was also presented [9]. Furthermore, Holden and

Erneux [10] and Smolen et al. [11] synchronously and autonomously researched the high-fade form of exploding, Class V, even though it was postulated in [12], and Rush and Rinzel [13] focused on the polygonal form of erupting, designated Category VI. Researchers have indeed shown that the exploding designation described previously is not very effective at differentiating between erupting varieties with minute differences. Izhikevich envisioned a far more thorough classification scheme predicated on the bifurcation principle of incredibly rapidly chaotic environments [14] to address this issue. This procedure includes key factors, coupled nonlinear conflation points, slide branching positions, and other bifurcation positions to locate the various exploding behaviours and manipulate them. The multiple forms of eruption discussed before, along with a substantial plethora of diverse varieties, are all identified by this new clustering algorithm. Izhikevich's method, for example, can be used to find sixteen different types of explosions in the most basic $(2 + 1)$ geometrical fast–low framework. In the context of extremely quickly chaotic environments, explosion is a fundamentally different temporal spectrum occurrence, and the transition between a dormant region and a monotonous stimulatory condition is caused by the slow attribute involved in regulating the high speed boosting [15].

Because the lipid bilayer of neurotransmitters is typically analogous to a bypass capacitor schematic illustration in electroencephalographic trials, bypass inductors and controller suppositions may be used to understand the explosion operation of a sensory organ [16]. In this regard, the fractional-order capacitance suggested by Westerlund and Ekstam [17] is profitable. Several studies [18–20] have discovered that this specific strain of inductors is critical in depicting the conductivity features of cellular membranes, hepatocytes, and connective tissue for prevailing perturbation by remembering the amplitude that was previously confined to. The fractional-order inductor, then, has traumatic memories. The index kernel is indeed a significant characteristic of fractional-order capacitors. In contrast to classical models, the index-kernel responds to abrupt signal transformation in a variety of neural circuitry, including neurogenesis interaction and developmental behaviour [21]. Certainly, research teams across a broad range of disciplines have been focusing their attention on fractional difference equations (FDEs). According to analysis, fractional calculus can generate a straightforward framework for the depiction of the interactive occurrences that take place in physiological organs and connective tissue and aid in comprehending the fundamental multi-scale mechanisms [19,22–26]. Notably, fractional calculus is crucial for comprehending the simple geometric characteristics of vesicles, synapse structures, and circuit design. As a result, this novel computational platform may support effective communication production, stimulation recognition, and intensity development stage transitions of oscillation neurotransmission [27,28].

To comprehend authentic nerve fibres with their increasing complexity and numerous exploding correlations, several neuron frameworks have indeed been put forth. The FitzHugh–Nagumo (FHN), Wilson–Cowan (WC) and Hindmarsh–Rose (HR) frameworks, as well as the Hodgkin–Huxley, are a few well-known representations that have undergone extensive research. Various versions have distinctive exploding correlations and characteristics. Undoubtedly, one of the most significant areas of study in the qualitative concept of fractional-order frameworks is stability interpretation. Notable surveys [29–31] provide comprehensive summaries of fractional-order structure stability analysis. Matignon's stability formula, which has been generalized in Sabatier and Farges [32], provides another very crucial basic foundation in the specific situation of sequential automated commensurate fractional-order mechanisms. Previous research has established linearization formalization (or generic versions of the conventional Hartman–Grobman formula) for fractional-order processes. Incommensurate order mechanisms have still not attracted the same level of interest as their commensurate order contemporaries

[33,34]. Petras [35] has been employed to analyse linear incommensurate fractional-order structures with rational orders. Numerous different projects have looked into perturbations in two-dimensional incommensurate fractional-order structures [36,37]. Trächtler [38] has recently focused on the BIBO consistency of mechanisms with irrational governing equations.

In this investigation, it was shown that an appropriate biophysical framework with elliptic erupting can be applied to analyse the fractional-order complexities of a confinement neuronal membrane. It regulates the speed of programming advancement via cell wall amplitude, which results in past history-dependent practices. Various configuration regimes with variously complex nonlinear characteristics are examined. In an attempt to acquire a reasonable overview of the impulse configurations and spike regularity in reliability and bifurcation contexts, this research examines the FHR neurotransmitter [39–41] in a fractional-order field. In numerical neuroscientific scripting, particularly in neurological scripting, the relationship between boosting and exploding is a pivotal issue in addition to an extremely interesting peculiarity. A frequent transformation between monotonous bursts and a dormant condition is presented by bursts. The vitality of the stimulation provided by the nonstationary circuit to the neuron determines the transitioning processes. The fact that the intensity of newly developing spiking interactions and discontinuing the boosting is not nonexistent, indicating that the vibrations may then have a comparatively tiny intensity, indicates that the trend of elliptic erupting will continue. This category of explosion was discovered through scientific investigation of rodent trifacial neurons that regulate mandibular mobility [42].

This has been discovered in the past: perhaps the slow parameter in the two-dimensional FHN approach provides a degree of mathematical challenge that enables chaos and other dynamical states for the membrane amplitude of the biological nerve cell. This has been discovered in the past: perhaps the slow parameter in the two-dimensional FHN approach provides a degree of mathematical challenge that enables chaos and other dynamical states for the membrane amplitude of the biological nerve cell. As a result, the fractional-order FHR biological neuron framework has an excellent contextual procedure for displaying a wide range of electrical impulse perturbations. For the asymptotic structural interpretation of the fractional-order commensurate FHR framework, necessary and sufficient requirements are examined. The quantifiable differences between the oscillation state and the dormant condition are displayed by bifurcation [43,44]. The fractional-order FHR framework is examined with a small selection of fixed specifications, and excessive numerical simplifications are generated for analysing the intrinsic behaviour analytically by utilizing the fractional-order as a core element. The result of this application of the integer-order system is biophysical diversity. We demonstrate how fractional-order complexities impact different assemblies of interacting oscillators' synchronization requirements. Different radiative behaviour that was not apparent in the integer-order system was ascertained when different fractional instructions were implemented.

Mathematical model

In 1965, the FHR framework, which is a modification of the conventional FHN neuron approach, was first invented by FitzHugh and Rinzel [39–41]. The fascinating physical and biological observations related to neurological excitability and spike formation are geometrically explained in the two-dimensional FHN system [45,46]. It displays an ongoing rise in response to a particular acute stressor. But it is unable to generate the many interesting fring structures made by neurogenesis. When certain specifications are diversified within a given time frame, the FHR neuron framework, a modified advanced variant of the FHN system, can generate a lot of fring behaviours. The framework is described by the incredibly fast control systems; the swift component uses the standard FHN formula. One component characterizes the slow

component. It is a general neural design that is algorithmically effective and biologically conceivable. The FHR system is described as follows:

$$
\begin{cases}
\dfrac{d\omega_1}{d\tau} = \omega_1 - \omega_1^3/3 - \omega_2 + \omega_3 + \mathcal{I}, \\[6pt]
\dfrac{d\omega_2}{d\tau} = \theta(\rho + \omega_1 - \varphi\omega_2), \\[6pt]
\dfrac{d\omega_3}{d\tau} = \varrho(v - \omega_1 - \zeta\omega_3),
\end{cases}
\tag{1}
$$

where ω_1, ω_2 and ω_3 stand for the membrane amplitude, the restoration parameter and the slow activation of the power supply. $\mathcal{I}$ ascertains the exogenous stimulation current's steady amplitude. Furthermore, ρ, φ, v, ζ and ϱ signifies the system parameters. The symbol ϱ denotes an affects the perception that controls how quickly the slow structure variable ω_3 changes. When θ is a small criterion, the fast component $(\omega_1 - \omega_2)$ displays a stress reduction oscillator in the transmission frequency. $m\omega_1$ (millivolt) scale is used to articulate ω_1. Time τ is measured in milliseconds (ms) [46]. For a specified point of $\mathcal{I}$, it displays stimulant activations or an undifferentiated situation contingent on the structural variables. The two-dimensional FHN model's variable ρ and the FHR neuron model's parameter v are equivalent. Reduced ρ results in sufficiently long pauses between two burstings, with a remarkably consistent period of erupting time. The interburst latencies shorten as ρ increases, and intermittent bursting transforms into stimulant spiking.

It was repeatedly explained how a concentrated impetus and membrane potential interact to produce an excitation capability, or significant rise. The non-ideal inductor controller illustrations can identify the impulse response, and the perfect restrictive concept identifies the neutral cell membrane dynamic system interpretation [47]. The membrane voltage behaviour is preserved by the hypothesis. It is crucial for understanding how the cell membranes behave when it comes to electricity [47]. Fractional-order complexities were discovered to adhere to a general power relevance in exploratory results [18]. It has been demonstrated that the power-law dynamics in neuronal thermal activity describe $\beta = 0.8$ for heat frog sciatic receptors and $\beta = 0.89$ for cold frog sciatic receptors, respectively. The fractional version presented as, $C\dfrac{d^\beta \omega_1}{d\tau^\beta} = \mathcal{I}$, which describes the non-ideal inductors supposition for the current–voltage connection, where $\beta \in (0,1)$. It has power complexities and maintains memory repercussions despite changes in membrane amplitude [48]. In the fractional-order situation, we take into account this juxtaposition. In narcolepsy, specific membrane modifications and membrane output current may trigger seizure-like activity [49]. In response to a particular stimulus's intensity, it might trigger muscular interactions. This kind of erupting occurrence can be studied more broadly to enable it to be applied to various scientific fields [50]. Let us investigate the fractional-order swift structure, which makes a significant contribution through diverse fring initiatives that emerge and vanish with changes in the fractional-order rationals and provides sophisticated fixed specifications.

The first order difference of the FHR system (1) is presented as follows:

$$
\begin{cases}
\Delta\omega_1(\mathbf{q}) = \omega_1(\mathbf{q}) - \omega_1^3(\mathbf{q})/3 - \omega_2(\mathbf{q}) + \omega_3(\mathbf{q}) + \mathcal{I}(\mathbf{q}), \\[4pt]
\Delta\omega_2(\mathbf{q}) = \theta(\rho + \omega_1(\mathbf{q}) - \varphi\omega_2(\mathbf{q})), \\[4pt]
\Delta\omega_3(\mathbf{q}) = \varrho(v - \omega_1(\mathbf{q}) - \zeta\omega_3(\mathbf{q})).
\end{cases}
\tag{2}
$$

The discrete fractional formulation for framework (2) is presented as follows:

$$
\begin{cases}
{}^c\Delta_\sigma^\beta \omega_1(\mathbf{q}) = \omega_1(\mathbf{q}+\beta-1) - \omega_1^3(\mathbf{q}+\beta-1)/3 \\
\qquad -\omega_2(\mathbf{q}+\beta-1) + \omega_3(\mathbf{q}+\beta-1) + \mathcal{I}(\mathbf{q}+\beta-1), \\[4pt]
{}^c\Delta_\sigma^\beta \omega_2(\mathbf{q}) = \theta(\rho + \omega_1(\mathbf{q}+\beta-1) - \varphi\omega_2(\mathbf{q}+\beta-1)), \\[4pt]
{}^c\Delta_\sigma^\beta \omega_3(\mathbf{q}) = \varrho(v - \omega_1(\mathbf{q}+\beta-1) - \zeta\omega_3(\mathbf{q}+\beta-1)),
\end{cases}
\tag{3}
$$

where $\beta \in (0,1]$, $\mathbf{q} \in \mathbb{N}_{\sigma+1-\beta}$, $\mathbb{N} = \{\sigma, \sigma+1, \sigma+2, \dots\}$ such that $\sigma \in \mathbb{R}$. In accordance [51], ${}^c\Delta_\sigma^\beta$ is the Caputo-like difference operator which is stated as

$$
{}^c\Delta_\sigma^\beta \chi(\mathbf{q}) = \Delta_\sigma^{-(\kappa-\beta)} \chi(\mathbf{q})
$$

$$
= \frac{1}{\Gamma(\kappa-\beta)} \sum_{v=\kappa}^{\mathbf{q}-(\kappa-\beta)} (\mathbf{q}-v-1)^{(\kappa-1-\beta)} \Delta^\kappa \chi(v),
\tag{4}
$$

where $\mathbf{q} \in (\mathbb{N})_{\sigma+\kappa-\beta}$ and $\kappa = \lceil\beta\rceil + 1$. Furthermore, the βth fractional sum which is mainly due to [52], defined as

$$
\Delta_\sigma^{-\beta} \chi(\mathbf{q}) = \frac{1}{\Gamma(\beta)} \sum_{v=\beta}^{\mathbf{q}-\beta} (\mathbf{q}-v-1)^{(\beta-1)} \chi(v), \quad \mathbf{q} \in (\mathbb{N})_{\beta+\kappa}, \ \beta > 0.
\tag{5}
$$

For $\beta = 1$, the memory kernel is unaffected, and the fractional-order framework operates in accordance with the integer-order approach. As we decline the fractional order from $\beta = 1$, the intermodulation distortion in the memory kernel intensifies, and the process models are time-dependent. This method is used to computationally consolidate the fractional-order FHR mechanism [50]. We have taken into account various kinds of parameters, including: $\rho = 0.7$, $\varphi = 0.8$, $\zeta = 1$, $\theta = 0.08$, $v = -0.775$ and $\varrho = 0.0001$. First, we choose $(\mathbf{r}_1)$: $\mathcal{I} = 0.3125$, $(\mathbf{r}_2)$: $\mathcal{I} = 0.4$. $(\mathbf{r}_3)$: $\mathcal{I} = 3$, $\varrho = 0.18$. $(\mathbf{r}_4)$: $\mathcal{I} = 0.3125$, $v = 1.3$, $\varrho = 0.0001$. $(\mathbf{r}_5)$: $v = -0.908$, $\varrho = 0.002, \mathcal{I} = 0.3125$ and the leftover factors are the same as above. We employ these predictor variables to analyse the FHR framework. The framework displays various fringing structures such as ellipsoidal erupting, tonic surging increasing, swift rocketing, and slightly elevated intensity solitary spikes with different vibration perturbations. The multiple ring patterns and configuration progressions are examined for appropriate parametric regimes that conform to the quantifiably distinct system dynamics of a neuron.

We will present the mathematical formula below, which facilitates us to obtain the quantitative strategy of the innovative fractional FHN discrete system (2), in order to analyse the intricacies of framework (2):

Theorem 1 ([53]). *The solution of the initial value problem (IVP)*

$$
\begin{cases}
{}^c\Delta_\sigma^\beta \chi(\mathbf{q}) = \mathbf{h}_1(\mathbf{q}+\beta-1, \chi(\mathbf{q}+\beta-1)), \\[4pt]
\Delta^\kappa \chi(\sigma) = \chi_\kappa, \quad \mathbf{n} = \lceil\beta\rceil + 1, \quad \kappa = 0,1,\dots,\mathbf{n}-1,
\end{cases}
\tag{6}
$$

is expressed a

$$
\chi(\mathbf{q}) = \chi_0(\sigma) + \frac{1}{\Gamma(\beta)} \sum_{v=\sigma+\mathbf{n}-\beta}^{\mathbf{q}-\beta} (\mathbf{q}-1-v)^{(\beta-1)} \mathbf{h}_1(v-1+\beta, \chi(v-1+\beta)), \quad \mathbf{q} \in \mathbb{N}_{\sigma+\mathbf{n}},
\tag{7}
$$

where

$$
\chi_0(\sigma) = \sum_{\kappa=0}^{\mathbf{n}-1} \frac{(\mathbf{q}-\sigma)^\kappa}{\Gamma(\kappa+1)} \Delta^\kappa \chi(\sigma).
\tag{8}
$$

Remark 1. *Letting $\sigma = 0$, since $(\mathbf{q}-1-v)^{(\beta-1)} = \dfrac{\Gamma(\mathbf{q}-v)}{\Gamma(\mathbf{q}+1-v-\beta)}$ and for $\ell = v + \beta - 1$ and $\mathbf{n} = 1$, the numerical technique (7) can be illustrated for $\beta \in (0,1]$ as follows*

$$
\chi(\mathbf{q}) = \chi(0) + \frac{1}{\Gamma(\beta)} \sum_{\ell=0}^{\mathbf{q}-1} \frac{\Gamma(\mathbf{q}-1-\ell+\beta)}{\Gamma(\mathbf{q}-1)} \mathbf{h}_1(\ell, \chi(\ell)).
\tag{9}
$$

This theorem leads to the numerical formulation for the discrete fractional FHR model (3), which is as follows:

$$
\begin{cases}
\omega_1(\mathbf{q}) = \omega_1(0) + \dfrac{1}{\Gamma(\beta)} \displaystyle\sum_{\ell=0}^{\mathbf{q}-1} \dfrac{\Gamma(\mathbf{q}-\ell-1+\beta)}{\Gamma(\mathbf{q}-1)} \\
\qquad \times \Big(\omega_1(\ell) - \omega_1^3(\ell)/3 - \omega_2(\ell) + \omega_3(\ell) + \mathcal{I}(\ell) \Big), \\[8pt]
\omega_2(\mathbf{q}) = \omega_2(0) + \dfrac{1}{\Gamma(\beta)} \displaystyle\sum_{\ell=0}^{\mathbf{q}-1} \dfrac{\Gamma(\mathbf{q}-\ell-1+\beta)}{\Gamma(\mathbf{q}-1)} \theta \\
\qquad \times \Big(\rho + \omega_1(\ell) - \varphi\omega_2(\ell) \Big), \\[8pt]
\omega_3(\mathbf{q}) = \omega_3(0) + \dfrac{1}{\Gamma(\beta)} \displaystyle\sum_{\ell=0}^{\mathbf{q}-1} \dfrac{\Gamma(\mathbf{q}-\ell-1+\beta)}{\Gamma(\mathbf{q}-1)} \varrho \\
\qquad \times \Big(v - \omega_1(\ell) - \zeta\omega_3(\ell) \Big), \quad \mathbf{q} = 1,2,\dots.
\end{cases}
\tag{10}
$$

Qualitative aspects of the FHR model

To govern the chaotic developments of the suggested fractional FHR system, we recommend a stabilization influence strategy in the subsequent paragraphs. Designing an efficient processing touchpad that causes all of the system's states to asymptotically strive towards zero is the aim of the stabilization influence scheme.

First of all, we examine the stability analysis of the proposed framework (2) as follows:

The f_p f_p of the model (2) are concluded as $\omega_2^* = \frac{\omega_1^* + \rho}{\varphi}$, $\omega_3^* = \frac{v - \omega_1^*}{\zeta}$ and $\omega_1^{*3} - 3\omega_1^* \wp_1 = \wp_2$, where $\wp_1 = \frac{\varphi\zeta - \zeta - \varphi}{\varphi\zeta}$ and $\wp_2 = 3\frac{\varphi\zeta\mathcal{I} - \rho\zeta + v\varphi}{\varphi\zeta}$, respectively. The framework (2) can also have up to three steady states depends entirely on the discriminant of the cubic polynomial $\mathcal{G}(\omega_1^*) = \omega_1^{*3} - 3\omega_1^* \wp_1 = \wp_2$.

Throughout this investigation, the presumption **(a)** $\varphi\zeta < \varphi + \zeta$ holds.

Theorem 2. *Suppose that there is a strictly nondecreasing mapping $\mathcal{G}(\omega_1^*)$ and there exists only one branch of steady states $E_1(\wp_2) = \left(\omega_1^*, \frac{\omega_1^* + \rho}{\varphi}, \frac{v - \omega_1^*}{\zeta}\right)$ having $\wp_2 \in \mathbb{R}$, for model (2), where $\omega_1^*(\wp_2) = \mathcal{G}^{-1}(\wp_2)$.*

Proof. By means of the given hypothesis, $\mathcal{G}(\omega_1^*) = \omega_1^{*3} - 3\omega_1^* \wp_1$ and $\mathcal{G}'(\omega_1^*) = 3\omega_1^{*2} - 3\wp_1$. Under the assertion **(a)**, the discriminant of $\mathcal{G}'$ is presented as $D(\mathcal{G}') = \frac{36(\varphi\zeta - \zeta - \varphi)}{\varphi\zeta}$, we find $D(\mathcal{G}') < 0$ that implies $\mathcal{G}'(\omega_1^*) > 0$ and the mapping $\mathcal{G}$ is strictly non-decreasing on $\mathbb{R}$. Therefore, it has unique real factor $\omega_1^*(\wp_2) = \mathcal{G}^{-1}(\wp_2)$. The Jacobian matrix of model (2) at the f_p $E_1(\omega_1^*, \omega_2^*, \omega_3^*)$ is presented by

$$\mathfrak{J}(\omega_1^*) = \begin{pmatrix} 1 - \omega_1^{*2} & -1 & 1 \\ \theta & -\theta\varphi & 0 \\ -\rho & 0 & -\rho\zeta \end{pmatrix}. \qquad (11)$$

The characteristic polynomial is

$$\begin{aligned} \mathcal{W}(\psi) = {} & \psi^3 - (1 - \omega_1^* - \theta\varphi - \rho\zeta)\psi^2 \\ & + (\theta - \theta\varphi + \rho - \zeta\rho + \varphi\zeta\rho + \varphi\theta\omega_1^{*2} + \zeta\rho\omega_1^{*2})\psi \\ & - (\varphi\zeta\theta\rho - \varphi\theta\rho - \zeta\theta\rho - \varphi\zeta\theta\rho\omega_1^{*3}). \end{aligned} \qquad (12)$$

In view of assertion **(a)** and $\det(\mathfrak{J}) = \rho\theta((\varphi\zeta - \varphi - \zeta) - \varphi\zeta\omega_1^{*2}) < 0$, we observe that one or more root of (12) is negative. Assuming the specific value of $\zeta = 1$ (which is fixed and remains constant model's specifications), we have $\mathcal{W}(-\rho) = \rho(\varphi\theta - \rho)$. When $\rho < \varphi\theta$ then $\mathcal{W}(-\rho) > 0$, which asserts that $\mathcal{W}(\psi)$ has one or more real factor that is located in $(-\infty, -\rho)$, therefore the factor is located in $[-\rho, 0)$. Following an analogous process, we can indeed obtain the analysis outcomes for the scenario when $\rho > \varphi\theta$. We should first describe the argument when $\rho < \varphi\theta$ for analytical intervention.

When the Jacobian matrix trace disappears, the solution was subjected a hopf bifurcation that alters its stability, that is., $1 - \omega_{1H} - \theta\varphi - \rho\zeta = 0$, yields $\omega_{1H} = -\sqrt{1 - \theta\varphi - \rho}$ (*say* β_1) and $\omega_{1H} = \sqrt{1 - \theta\varphi - \rho}$ (*say* β_2). The framework parameter designated as ω_{1H} is where hopf bifurcation takes place. $\square$

Theorem 3. *Suppose the steady states $E_1(\wp_2)$ of model (2) is asymptotically stable (without regard to the fractional-order, β) for each $\mathcal{G}(\beta_1) \geq \wp_2$ or $\mathcal{G}(\beta_2) \leq \wp_2$.*

Proof. Assume that we implement the scenario where $\mathcal{G}(\beta_1) \geq \wp_2$, then $\omega_1^* = \omega_1^*(\wp_2) = \mathcal{G}^{-1}(\wp_2) \leq \beta_1 < 0$. Moreover, if $\mathcal{G}(\beta_2) \leq \wp_2$, then $\omega_1^* = \omega_1^*(\wp_2) = \mathcal{G}^{-1}(\wp_2) \geq \beta_2$. In both instances, this is attainable $\mathcal{W}(1 - \rho - \theta\varphi - \omega_1^{*3}) < 0$. Therefore, the negative real root (*say* ψ_1) of $\mathcal{W}(\psi)$ located in $(1 - \rho - \theta\varphi - \omega_1^{*3}, \rho)$ and in addition to the remaining two roots $\psi_2 + \psi_3 = 1 - \rho - \theta\varphi - \omega_1^{*3} - \psi_1 < 0$ and $\psi_2\psi_3 = \det(\mathfrak{J})/\psi_1 > 0$, respectively. According to the clarification above, the steady state $E_1(\wp_2)$ is asymptotically stable and free of the fractional-order because the roots are located on the negative real axis. $\square$

Theorem 4. *If $\wp_2 \in (\mathcal{G}(\beta_1), \mathcal{G}(\beta_2))$, then the steady state of the model (2) is asymptotically stable if and only if $(1 - \omega_1^{*3} - \theta\varphi - \rho - \psi_1)\sqrt{-\psi_1} < 2\sqrt{-\det(\mathfrak{J})}\cos(\beta\pi/2)$, or correspondingly,*

$$\beta < 0.6366197 \arccos\left(\min\left(1, \max\left(0, \frac{(1 - \omega_1^{*3} - \theta\varphi - \rho - \psi_1)\sqrt{-\psi_1}}{2\sqrt{-\det(\mathfrak{J})}}\right)\right)\right), \qquad (13)$$

where $\psi_1 = \psi_1(\wp_2) \in (-\infty, -\rho)$ is the smallest root of (12).

Proof. The smallest root, as we have previously demonstrated, $\psi_1 = \psi_1(\wp_2) \in (-\infty, -\rho)$ in addition the remaining roots of $\mathcal{W}(\psi)$ holds $\psi_2 + \psi_3 = 1 - \omega_1^{*3} - \theta\varphi - \rho - \psi_1$, $\psi_2\psi_3 = \det(\mathfrak{J})/\psi_1 > 0$. Presently, the roots ψ_2 and ψ_3 meet the requirement for asymptotic stability assumption $|\arg(\psi)| > 1.57079\beta$ if and only if $\psi_2\psi_3 > 0$ and $(\psi_2 + \psi_3)/\sqrt{\psi_2\psi_3} < 2\cos(1.57079\beta)$ satisfies. Using the significance of $\psi_2 + \psi_3$ and $\psi_2\psi_3$, we are able to derive the requirement (13). $\square$

Bifurcation analysis

Utilizing the MATLAB software, the bifurcation interpretation for the FHR framework of integer-order is carried out. Including $\rho = 0.0002$, the implemented stimulation $\mathcal{I}$ is addressed as the dominant criterion, while the remaining factors are adjusted to their default configuration.

Remarkably hopf bifurcations at $\mathcal{I} = 0.147523$ and $\mathcal{I} = 1.000009$ cause the subthreshold state to vanish (see; Fig. 1). The steady state region is symbolized above the dotted blue line in the Fig. 1(a) and (b), whereas the unsteady state is represented below the dotted blue line in the Fig. 1(a) and in Fig. 1(b), respectively. In both cases, $\mathcal{I} < 0.147523$ and $\mathcal{I} > 1.000009$, the framework has a stable focus node. The scheme has saddle foci for the wavelengths $0.147523 < \mathcal{I} \leq 0.7$ and $0.000234 < \mathcal{I} \leq 1.000009$, respectively. At $\mathcal{I} = 1.000009$ (choose $\mathcal{I}$) [42], the FHR system exhibits elliptic spurting; moreover, as we boost $\mathcal{I} \in (0.4, 0.7]$, it exhibits the commonality of frequent spiking and exploding. Additionally, the information presents consistent spikes as $\mathcal{I}$ rises. The framework has a saddle point for $\mathcal{I} \in (0.7, 1.0]$. In this domain, it first exhibits frequent boosting before exhibiting the first impulse delay as $\mathcal{I}$ increases. The framework initially displays frequent boosting as first impulse connectivity for $\mathcal{I} \in (0.000234, 1.00009]$, but as $\mathcal{I}$ increases, it displays anomalous spurting for first impulse propagation delay. The Fig. 1(a) denotes an unsteady restriction spiral, while the Fig. 1(b) indicates a steady limit vicious circle. In the scenario of the fractional-order approach, the proximity strategies of the hopf bifurcation are taken into account as the system's findings. In the integer-order scheme, Andronov–hopf bifurcation demonstrates the local conception as well as the fatality of the intermittent solution. The indication of the component $\mathbf{n}_\iota(\beta, \mathcal{I}) = 1.57079\beta - |\arg(\psi_\iota)|$, $\iota = 1, 2, 3$ establishes the consistency of the fractional-order framework all over such a equilibrium state. Within the steady state, the framework is declared stable or unstable if $\mathbf{n}_\iota(\beta, \mathcal{I}) < 0$ or $\mathbf{n}_\iota(\beta, \mathcal{I}) > 0$. In the integer-order framework, the factor $\mathbf{n}_\iota(\beta, \mathcal{I})$ operates similarly to the real portion of the characteristic value. As a result, the prerequisite for hopf-bifurcation to eventually happen in a fractional-order mechanism is:

(i) For two complex-conjugate characteristic values and a real characteristic value, then matrix $\mathfrak{J}$ has the following assumption $D(\mathcal{W}(\mathcal{I}^*)) < 0$, where the significance level of the dominant criterion is $\mathcal{I}^*$.

(ii) $\mathbf{n}_\iota(\beta, \mathcal{I}^*) = 0$ and $\psi_3(\mathcal{I}^*) \neq 0$.

(iii) $\left.\partial\mathbf{n}/\partial\mathcal{I}\right|_{\mathcal{I} = \mathcal{I}^*} \neq 0$.

When the component $\mathcal{I}$ in the mechanism (2), the hopf bifurcation takes place $\mathcal{I} \in (0.000234, 1.00009)$. Plot 1 depicts the stable/unstable domain for steady state $E_1(\wp_2)$ with criterion frames **(i)** and **(ii)** in the $(\mathcal{I}, \beta)$-plane, respectively. The critical values β^* provided by the
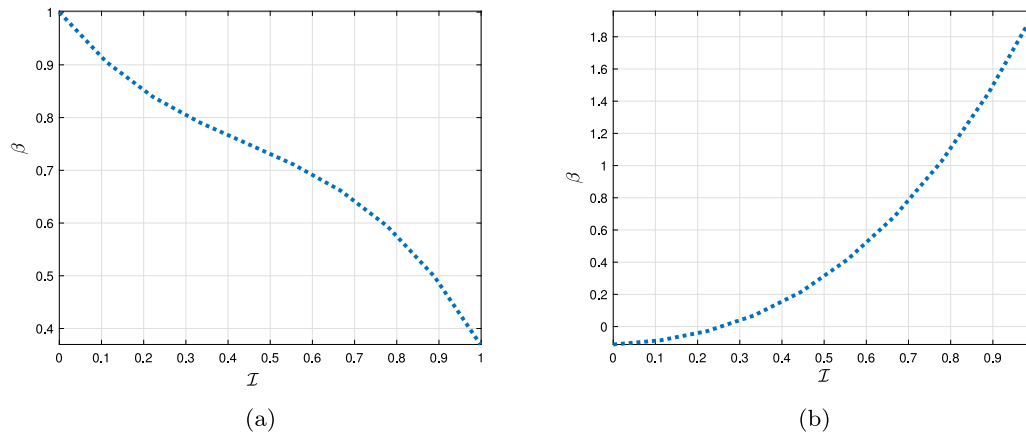
Fig. 1. For criterion sets ($\mathbf{r}_1$) and ($\mathbf{r}_2$), respectively, the bifurcation consequences of the FHR model (2) are schemed.

formula deduced from $\mathbf{n}_i(\beta, \mathcal{I}^*) = 0$ are represented by the graph as the hopf bifurcation plot. Choosing $\mathcal{I} = 0.000234$, then the critical value is $\beta^*(0.000234) = 0.28016$. When $\beta < \beta^*(0.000234)$, the framework (2) is asymptotically stable. When $\beta > \beta^*(0.000234)$, it is unstable. The hopf bifurcation is present in the system (2) for $\beta = \beta^*(0.000234)$. For the numerical analyzation, we did not take into account the domain $\mathcal{I} \in [0.000234, 1.00009]$ because $D_1(\mathcal{W}(\mathcal{I})) > 0$. For the majority of attributes of the fractional-order, the system state is asymptotically stable; however, for a relatively small possible value systems of β, it is unpredictable. The corresponding values for the hopf bifurcation for $\mathcal{I} = 0.3897$ is $\beta^*(0.5) = 0.80000$.

Acknowledging the singularity methodology of these exploding forms is aided by the process depictions demonstrated in Fig. 2, where Fig. 2 is applicable to the situation in Fig. 1 in which there is a threshold instability process in a steady state. As shown in Fig. 2(a)–(q), the hopf bifurcation at **(i)**, **(ii)** and **(iii)**, the comparatively small amplitude around the steady state, is relevant to the situation depicted in Fig. 1.

Commensurate fractional FHR system

Presently, we evaluate diverse fring initiatives using the fractional-order FHR neuron framework. With regard to reliability and bifurcation analyzation for various orders, we assess how the integer-order complexity adjusts its neurogenesis behaviour and how exploding modifications affect different fring structures. For the simulation solution, the time phase $\Delta = 0.1$ was employed. For all of the simulation studies, we treated the ICs as minor irregular deviations from the f_p. Now, a homogeneously disseminated spontaneous quantity in the time-frame serves as the source of the spontaneous fluctuation of $(0, 1)$. The classical FHR framework yields elliptic spurting now at configuration designated ($\mathbf{r}_1$), which is an intriguing component. Even during passive process of overflowing, it produces pulsations with small amplitudes that deteriorate and expand but are not quickly dampened. According to the fring structure (see; Fig. 3(a)), there are numerous varieties of stems within every spurt and several switching frequency instabilities between two discharges. Even if we drastically reduce the fractional order from $\beta \in (0, 1)$, the effective and motionless steps of erupting transformation remain. At $\beta = 0.95$, it exhibits quick boosting; however, after a while, it produces mingled perturbations to heightened sensitivity solitary boosting and low spectral vibrations (see; Fig. 3(b)). Besides reducing it to $\beta = 0.85$ (see; Fig. 3(c)), it only diverse applications fluctuations. The discrete fractional interactive content a hopf bifurcation at $\beta = 0.80828$ and enters a subthreshold regime when $\beta < 0.80828$, or when it accumulates to the steady f_p ($\omega_1^* = 0.795467$) at $\beta = 0.75$ (see; Fig. 3(d)).

We currently surmise the criteria specified in ($\mathbf{r}_2$). The tonic surge in the classical order approximation is depicted in Fig. 3. When $\beta = 0.95$, the fractional-order changes from tonic excitability to a different stimulatory configuration with elevated impulse response and high-frequency vibrations (see; Fig. 3(e)). At $\beta = 0.85$, the process presents mingled fluctuations (see; Fig. 3(f)). When the framework is in this transfer configuration, there is a first bump delay and the fring intensity drops. At this point, the interactive content reaches a hopf bifurcation and enters a comprehensive subthreshold condition, as illustrated in Fig. 3(g), (where $\omega_1^* = -0.79534$ and $\beta = 0.65$). Beside that, using configuration plan ($\mathbf{r}_3$), the classical order excitatory version generates yet a further stimulatory structure (see; Fig. 3(h)). In contrast to the conventional framework, it exhibits minimal operating intensity growths at $\beta = 0.99$ and exhibits first slight bump response time (see; Fig. 3(i)). Additionally, it reaches a point of quiescence at $\beta = 0.93$ (see; Fig. 3(j)). The process furthermore reaches a reliable f_p at this location ($\omega_1^* = 0.79236$). We then take into account criterion specify ($\mathbf{r}_4$). According to Fig. 3, the integer-order approach exhibits fast-spiking. Then, first it exhibits mingled perturbations before shooting up regularly at $\beta = 0.85$ (see; Fig. 3(k)). The structure experiences its first impulse transmission delay as fractional-orders and band intensity reduction. As the fractional-order $\beta = 0.90$ is reduced, the system's first oscillations response time rises (see; Fig. 3(l)). The configuration plan ($\mathbf{r}_5$) has now been taken into consideration. According to the integer-order framework, perturbations of low displacement do not entirely deteriorate to a motionless process or oscillatory destruction (see; Fig. 3(m)). With $\beta = 0.96$, the time frame of different amplitude vibrations increases with decreasing fractional order, decreasing signal incidence, and rapidly expanding with a longer moment time frame (see Fig. 3(n)). At $\beta = 0.97$, the structure corresponds to the robust f_p ($\omega_1^* = -0.86594$), and then it enters the comprehensive inactive process (see; Fig. 3(o)).

Here, we use predictability and bifurcation interpretation to describe these specific neuronal reactions. The findings demonstrate that at $\beta = 1$, the ω_1-memory pattern is nonexistent. The complexities of the mechanism at $\beta = 1$ are unaffected by the memory feature (see; Fig. 3(p)). Different dynamic system interactions appear when fractional order is reduced relative to integer order. The filtration voltage complexities are significantly impacted by the voltage memory feature, and the memory sequence is also significantly impacted by filtration amplitude (see; Fig. 3(p)). At relatively limited fractional-orders, the fractional-order process is relatively constant for all structural factors, meaning that the procedural memory gets too modest and is unable
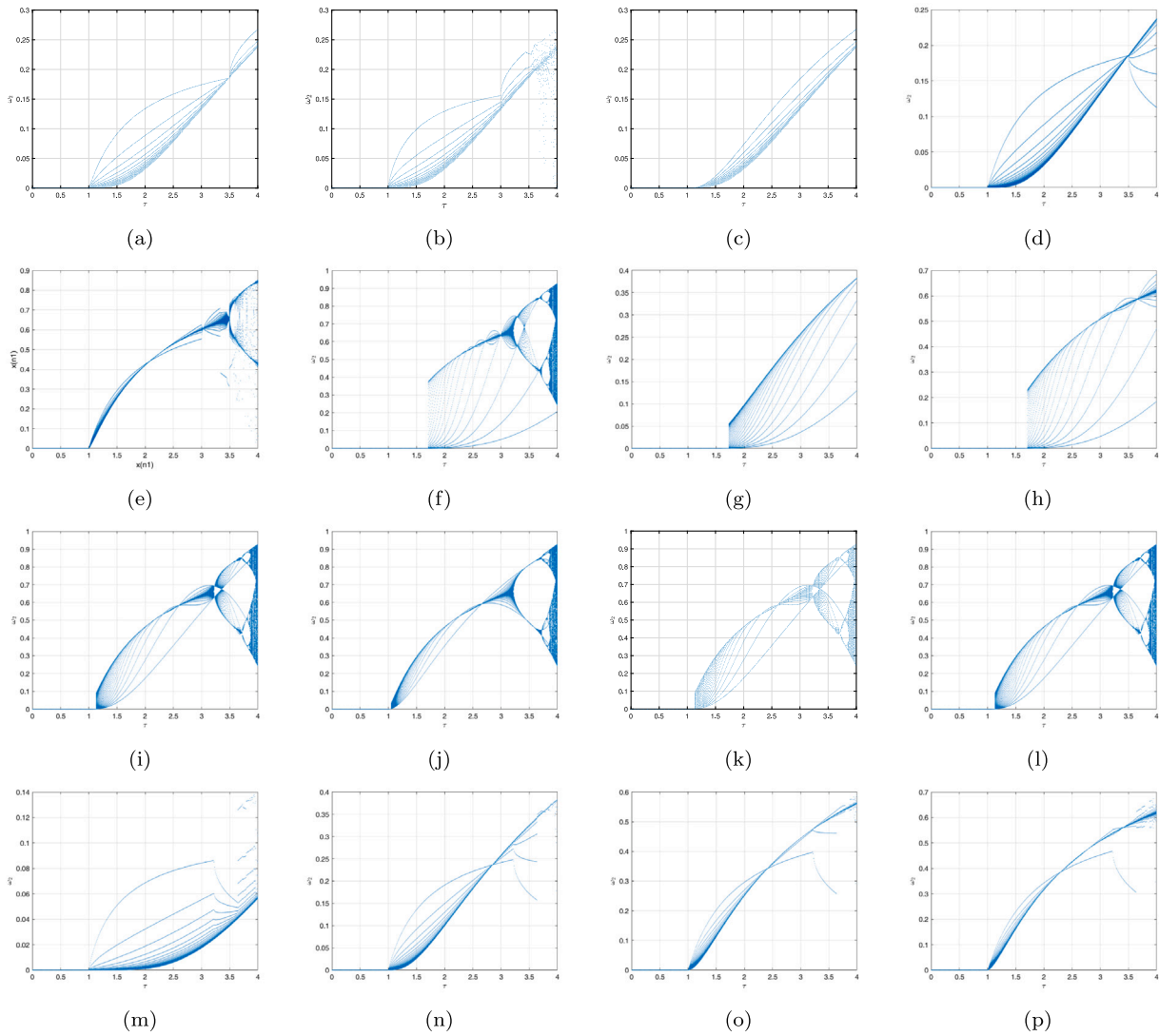
Fig. 2. Bifurcation of FHR model (2) versus sets $(\mathbf{r}_1)$, $(\mathbf{r}_2)$, $(\mathbf{r}_3)$ and $(\mathbf{r}_4)$, respectively.

to have a serious influence on the filtration voltage interactions to cause a sharp rise (see; Fig. 3(p)). Therefore, as it starts to rise above a predefined criterion for a fixed list of parameters, the fractional-order excitatory controller produces varying perturbations.

Incommensurate fractional FHR system

This segment investigates the behavioural patterns of the discrete FHR system with non-commensurate fractional order expectations. The concept of employing different fractional orders for every formula in the structure is known as the "incommensurate order system". The following is a representation of the incommensurate fractional discrete FHR system:

$$
\begin{cases}
{}^{c}\Delta_{\sigma}^{\beta_1}\omega_1(\mathbf{q}) = \omega_1(\mathbf{q}+\beta_1-1) - \omega_1^3(\mathbf{q}+\beta_1-1)/3 - \omega_2(\mathbf{q}+\beta_1-1) \\
\qquad\qquad +\omega_3(\mathbf{q}+\beta_1-1) \\
\qquad\qquad +\mathcal{I}(\mathbf{q}+\beta_1-1), \quad \mathbf{q}\in\mathbb{N}_{\sigma_1+1-\beta_1} \\
{}^{c}\Delta_{\sigma}^{\beta_2}\omega_2(\mathbf{q}) = \theta(\rho+\omega_1(\mathbf{q}+\beta_2-1)-\varphi\omega_2(\mathbf{q}+\beta_2-1)), \quad \mathbf{q}\in\mathbb{N}_{\sigma_1+1-\beta_2} \\
{}^{c}\Delta_{\sigma}^{\beta_3}\omega_3(\mathbf{q}) = \varrho(\upsilon-\omega_1(\mathbf{q}+\beta_3-1)-\zeta\omega_3(\mathbf{q}+\beta_3-1)), \quad \mathbf{q}\in\mathbb{N}_{\sigma_1+1-\beta_3}.
\end{cases}
$$
(14)

In view of Theorem 1, the numerical representation of the incommensurate fractional discrete system (14) is delivered as

$$
\begin{cases}
\omega_1(\mathbf{q}) = \omega_1(0) + \dfrac{1}{\Gamma(\beta_1)}\displaystyle\sum_{\ell=0}^{\mathbf{q}-1}\dfrac{\Gamma(\mathbf{q}-\ell-1+\beta_1)}{\Gamma(\mathbf{q}-1)} \\
\qquad \times\Big(\omega_1(\ell) - \omega_1^3(\ell)/3 - \omega_2(\ell) + \omega_3(\ell) + \mathcal{I}(\ell)\Big), \\
\omega_2(\mathbf{q}) = \omega_2(0) + \dfrac{1}{\Gamma(\beta_2)}\displaystyle\sum_{\ell=0}^{\mathbf{q}-1}\dfrac{\Gamma(\mathbf{q}-\ell-1+\beta_2)}{\Gamma(\mathbf{q}-1)}\theta \\
\qquad \times\Big(\rho+\omega_1(\ell) - \varphi\omega_2(\ell)\Big), \\
\omega_3(\mathbf{q}) = \omega_3(0) + \dfrac{1}{\Gamma(\beta_3)}\displaystyle\sum_{\ell=0}^{\mathbf{q}-1}\dfrac{\Gamma(\mathbf{q}-\ell-1+\beta_3)}{\Gamma(\mathbf{q}-1)}\varrho \\
\qquad \times\Big(\upsilon-\omega_1(\ell) - \zeta\omega_3(\ell)\Big), \quad \mathbf{q}=1,2,\dots.
\end{cases}
$$
(15)

The specifications $\mathbf{r}_1 - \mathbf{r}_4$ are varied in the bifurcation diagrams in Fig. 4 to reveal the dynamic behaviour (14). It is obvious to see that the discrete incommensurate fractional FHR model (14) is affected by changes in orders β_1, β_2 and β_3, respectively. For example, we can be certain that the chaotic zone expanded when we fixed $\beta_2 = 1$ and boosted β_1 from 0.1 to 1, and that it decreased when we fix $\beta_1 = 0.95$ and significantly improved β_2 from 0.85 to 1. Besides that, as the mechanism criterion rises, the incommensurate map's dynamics steadily
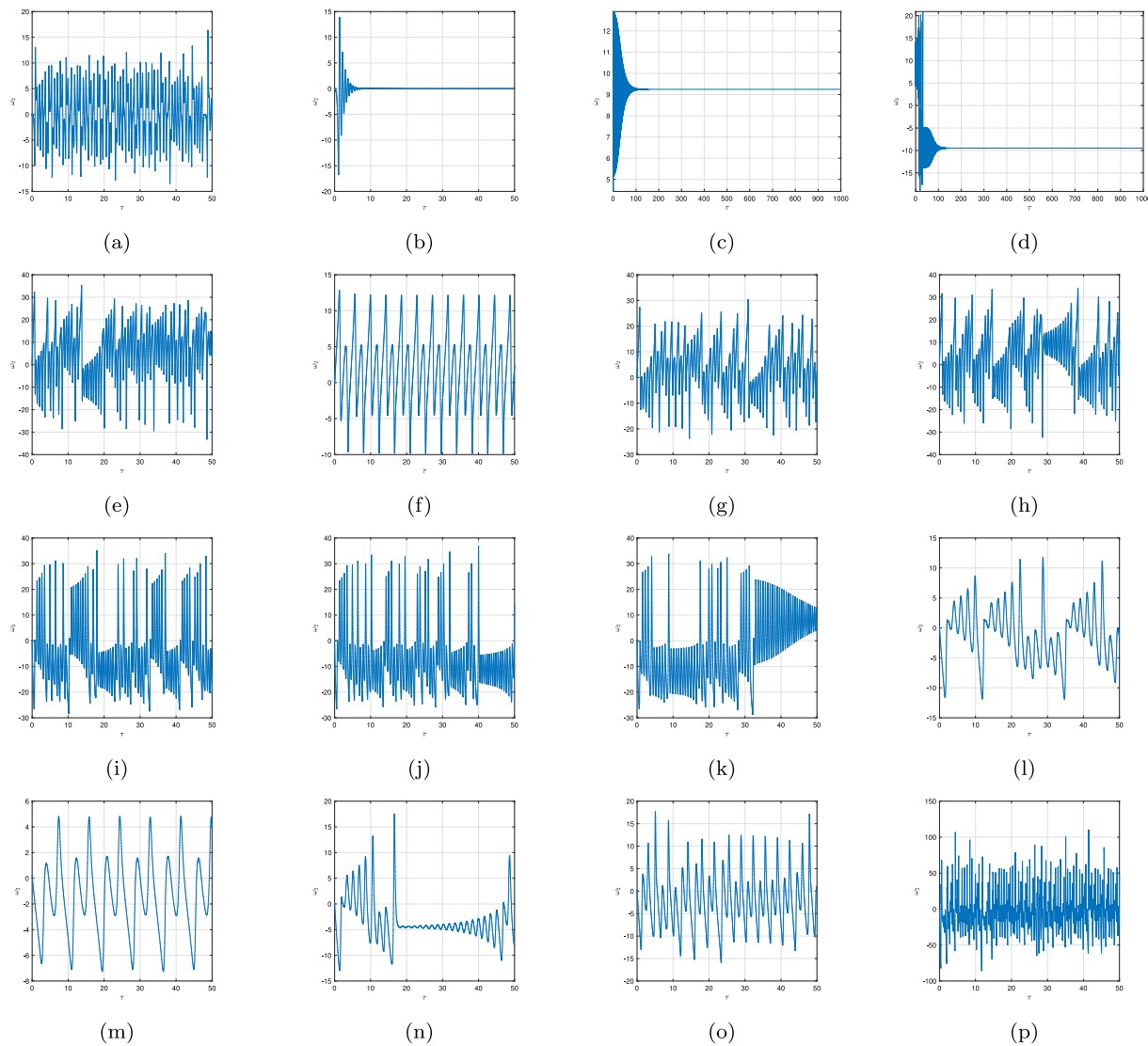
Fig. 3. Diverse neurological reaction of membrane amplitude (ω_1) for the discrete FHR system (2). 1st presentation: (a)–(d) for $\beta = 1.00, 0.95, 0.85$ and 0.75 (set $\mathbf{r}_1$). 2nd presentation: (e)–(h) for $\beta = 1, 0.95, 0.85$ and 0.75 (set $\mathbf{r}_2$). 3rd presentation: (i)–(l) for $\beta = 1.00, 0.95, 0.85$ and 0.75 (set $\mathbf{r}_3$). 4th presentation: (m)–(p) for $\beta = 1.00, 0.95, 0.85$ and 0.75 (set $\mathbf{r}_4$).

transform via a time frame branching from regular intervals asserting either a chaotic or a linear trajectory. Additionally, in an attempt to offer a better representation of the impact of incommensurate orders on the tendencies of the discrete fractional FHR model (14), we evaluate the two additional occurrences:

Case I: We change the order β_1 from 0.4 to 1 with $\Delta\beta_1 = 0.003$ scale factor. Fig. 4(a)–(d) shows the phase portraits and associated attribute values defined in set ($\mathbf{r}_1$) when $\beta_2 = 0.85$. As shown by productive set values ($\mathbf{r}_1$) in Fig. 4(e)–(h), it is obvious from Fig. 4 that the regime of the incommensurate game board (14) exhibits a dynamic nature for significantly bigger β_1 attributes. According to this finding, a slight periodic region is visible for $\beta_1 \in [0.3, 0.85]$. The incommensurate fractional representation also has a highly complicated chaotic attractor, which dramatically influences the complexities of the membrane amplitude, causing a sharp rise in their highest attributes as β_1 increases and approaches 1.

Case II: The phase portraits and its membrane voltage are attracted for β_1 to analyse the dynamical properties of the incommensurate fractional discrete FHR model (14) when $\beta_3 = 1$ is an adjustable criterion, as shown in Fig. 4(i)–(l). We can see that the paths deviate significantly towards infinity when the order β_2 has poor accuracy. Chaotic behaviours can be acquired when $\beta_2 \in [0.5, 0.95]$. Furthermore,

as β_2 approaches 1, the membrane voltage changes dramatically, indicating that the discrete incommensurate fractional FHR Eq. (14) is steady and has periodic panels. These results show that the nonlinear features of a fractional discrete FHR (14) depend on modifications in the incommensurate orders. Fig. 4(m)–(p) depictions of the model parameters of the incommensurate fractional system (14) reinforce the notion that the mechanism's behaviours may be appropriately represented by incommensurate orders.

Synchronization scheme

We take into account two inhibitory interneurons interacting with FHR neurons in the fractional field to investigate the complexities of the associated FHR receptors. According to connecting configuration and resilience, postsynaptic membrane interacting excitatory cells generate high levels of in-phase or anti-phase instantaneous interaction. We demonstrate the interacting fractional-order excitatory receptors' progressions towards the comprehensive synchronization (CS) restrictions [54]. We employ a structurally and functionally effective synaptic interfacial methodology called "bidirectional convolution", which is a high-voltage connection between two FHR neural connections. The goal of the synchronization procedures is to attempt to influence the
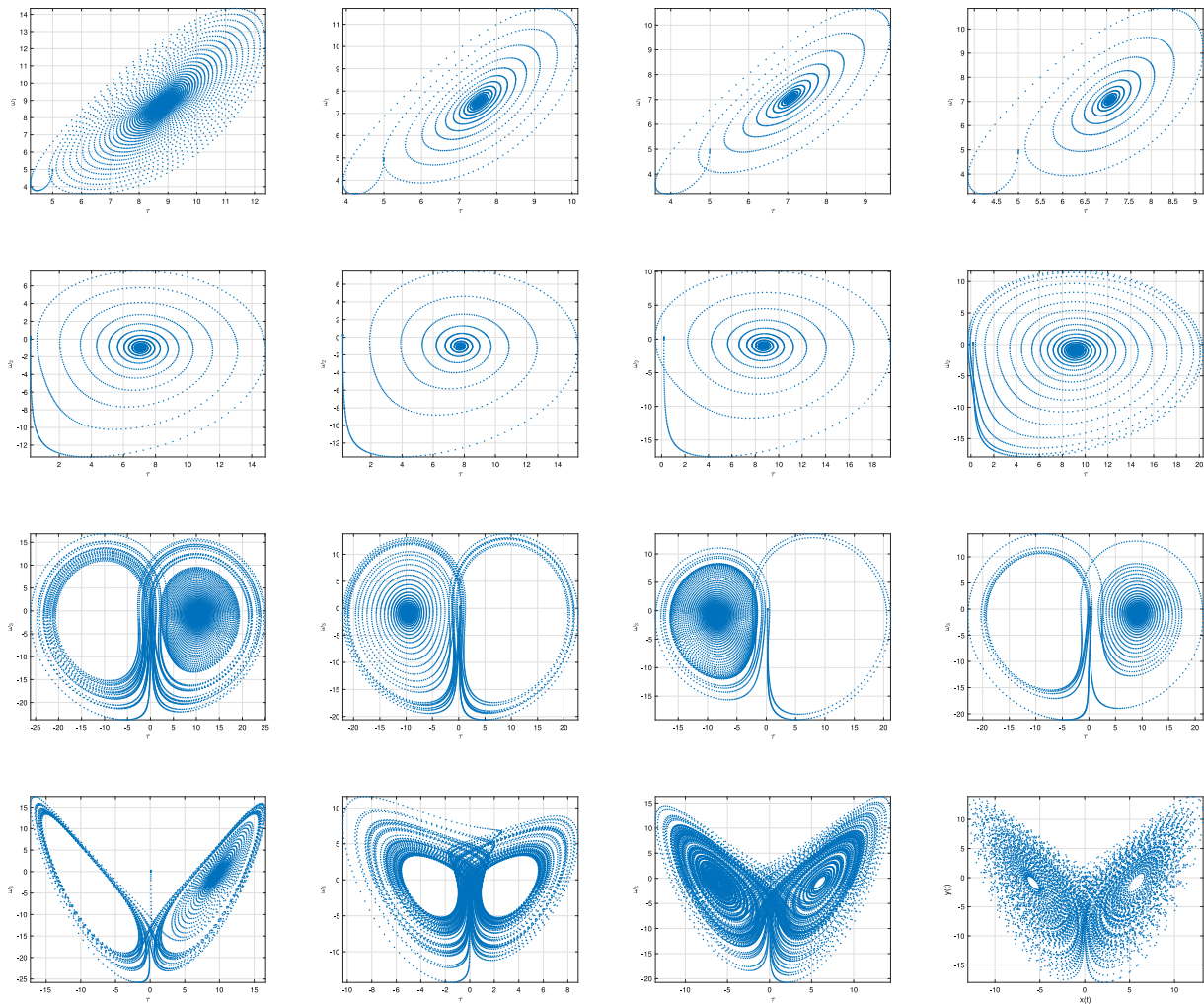
Fig. 4. Phase portraits of (14) for (set $(\mathbf{r}_1) - (\mathbf{r}_4)$) and with multiple fractional-orders $(\beta_1, \beta_2) = (0.75, 0.85)$, $(\beta_2, \beta_3) = (0.85, 0.95)$, $(\beta_1, \beta_3) = (0.85, 0.95)$, $(\beta_1, \beta_3) = (0.95, 0.1)$.

inaccuracy between the central controller and slave framework to congregate towards zero. The equivalent fractional FHR discrete system (2) shall be referred to as the main server, and the slave scheme shall be referred to as

$$
\begin{cases}
{}^c\Delta^\beta_\sigma \omega_{1_s}(\mathbf{q}) = \omega_{1_s}(\mathbf{q}+\beta-1) - \omega_{1_s}^3(\mathbf{q}+\beta-1)/3 - \omega_{2_s}(\mathbf{q}+\beta-1) + \omega_{3_s}(\mathbf{q}+\beta-1) \\
\qquad\qquad + \mathbf{h}_{e_1}(\omega_{1_j}(\mathbf{q}+\beta-1)) - \omega_{1_s}(\mathbf{q}+\beta-1) + \mathcal{U}_1(\mathbf{q}+\beta-1), \\
{}^c\Delta^\beta_\sigma \omega_{2_s}(\mathbf{q}) = \theta(\rho + \omega_{1_s}(\mathbf{q}+\beta-1) - \varphi\omega_{2_s}(\mathbf{q}+\beta-1)) + \mathcal{U}_2(\mathbf{q}+\beta-1), \\
{}^c\Delta^\beta_\sigma \omega_{3_s}(\mathbf{q}) = \varrho(\upsilon - \omega_{1_s}(\mathbf{q}+\beta-1) - \zeta\omega_{3_s}(\mathbf{q}+\beta-1)) + \mathcal{U}_3(\mathbf{q}+\beta-1),
\end{cases}
$$

(16)

where the mappings $\mathcal{U}_1$, $\mathcal{U}_2$ and $\mathcal{U}_3$ are synchronization controllers. The fractional error estimates are presented as

$$
\begin{cases}
{}^c\Delta^\beta_\sigma e_1(\mathbf{q}) = \omega_{1_s}(\mathbf{q}+\beta-1) - \omega_{1_s}^3(\mathbf{q}+\beta-1)/3 - \omega_{2_s}(\mathbf{q}+\beta-1) + \omega_{3_s}(\mathbf{q}+\beta-1) \\
\qquad\qquad + \mathbf{h}_{e_1}(\omega_{1_j}(\mathbf{q}+\beta-1)) - \omega_{1_s}(\mathbf{q}+\beta-1) + \mathcal{U}_1(\mathbf{q}+\beta-1) \\
\qquad\qquad - \Big\{ \omega_1(\mathbf{q}+\beta-1) - \omega_1^3(\mathbf{q}+\beta-1)/3 - \omega_2(\mathbf{q}+\beta-1) + \omega_3(\mathbf{q}+\beta-1) \Big\}, \\
{}^c\Delta^\beta_\sigma e_2(\mathbf{q}) = \theta(\rho + \omega_{1_s}(\mathbf{q}+\beta-1) - \varphi\omega_{2_s}(\mathbf{q}+\beta-1)) + \mathcal{U}_2(\mathbf{q}+\beta-1) \\
\qquad\qquad - \Big\{ \theta(\rho + \omega_1(\mathbf{q}+\beta-1) - \varphi\omega_2(\mathbf{q}+\beta-1)) \Big\}, \\
{}^c\Delta^\beta_\sigma e_3(\mathbf{q}) = \varrho(\upsilon - \omega_{1_s}(\mathbf{q}+\beta-1) - \zeta\omega_{3_s}(\mathbf{q}+\beta-1)) + \mathcal{U}_3(\mathbf{q}+\beta-1) \\
\qquad\qquad - \Big\{ \varrho(\upsilon - \omega_1(\mathbf{q}+\beta-1) - \zeta\omega_3(\mathbf{q}+\beta-1)) \Big\},
\end{cases}
$$

(17)

where $\mathbf{h}_{e_1}$ is the crosslinking intensity for $\iota = 1, 2$ and $j = 2, 1$, respectively. The membrane electric field provides a multiplexed coupling for the aforementioned mechanism. Resemblance processes are used to investigate the synchronization frameworks and their predictability. Comprehensive synchronization of these capacitive and inductive processes suggests that the inaccuracy system's zero solutions are stable [52,55]. Utilizing adequate conductivity potentials and acceptable fractional exponents at various parametric configurations, the intended synchronization behaviour is accomplished (see; Fig. 5(a)–(c)). Presently, in order to assess the synchronization inaccuracy seen between interacting neural circuits oscillators and generate CS, we implement a measurable statistic identified as the clustering algorithm. The mapping is described as

$$
S^2(\eta) = \frac{\langle \left(\omega_1(\tau) - \bar{\omega}_1(\tau - \eta) \right)^2 \rangle}{\left(\langle \omega_1^2(\tau) \rangle \langle \bar{\omega}_1^2(\tau) \rangle \right)^{1/2}}.
$$

(18)

where $S(\eta)$ represents the process delay observed between interacting excitatory mechanisms. The small displacement of $S(0)$ indicates a significant relationship between the operator and the feedback resonator. Despite the fact that the functional value $S(0)$ remains constant under various ICs, the CS mechanism is confirmed (see; Fig. 5(d)–(i)). This confirmed the effectiveness of the synchronization mechanism and the interference strategy.
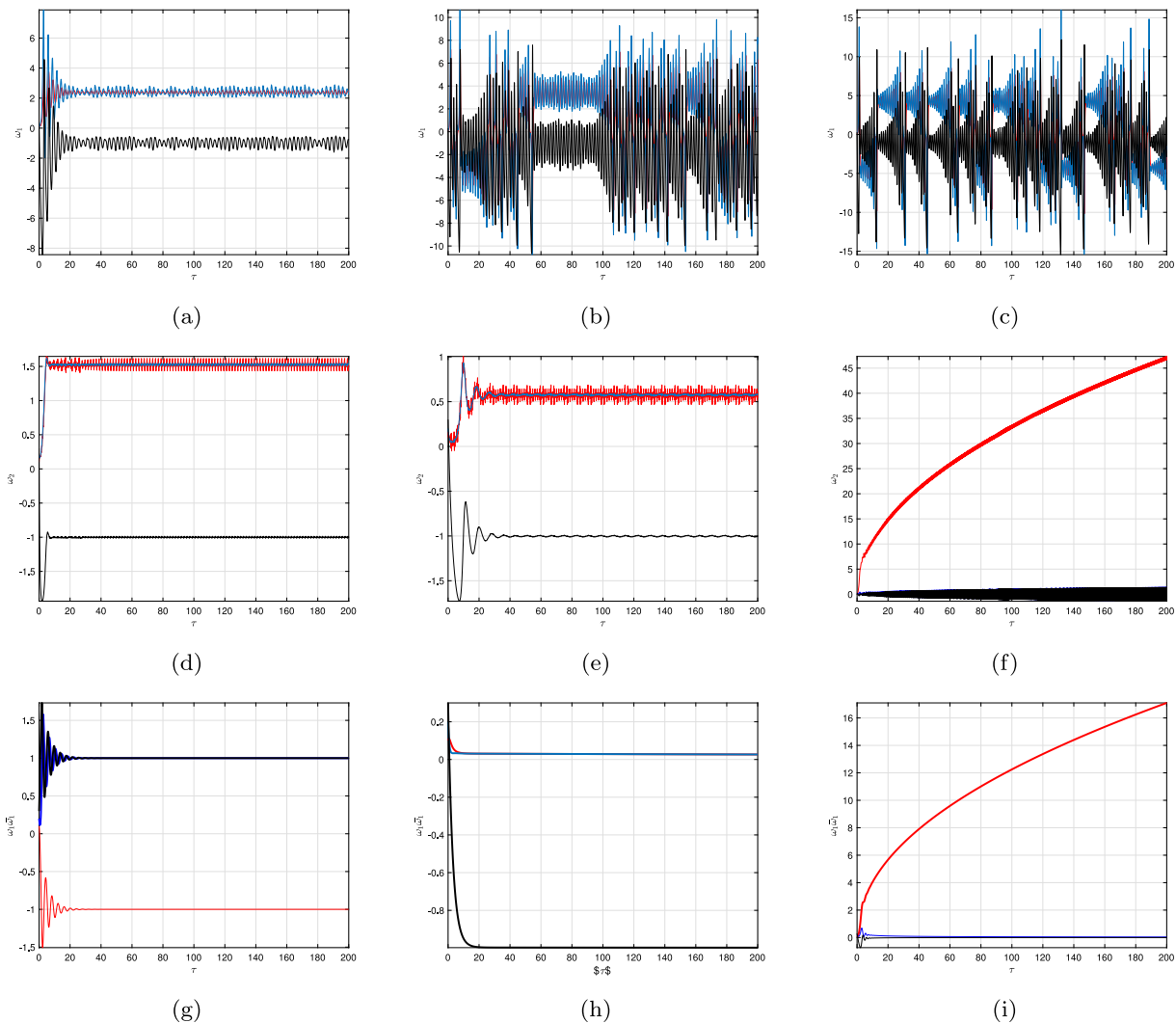
Fig. 5. The membrane combinations for configurations r_1 and r_2 correspond to the excitatory associated fractional FHR framework's high voltage crosslinking abilities of (a) $h_{e_1} = 0.57$ and (b) $h_{e_1} = 0.3$, respectively, at $\beta = 0.95$. Compare ω_1 and $\bar{\omega}_1$ for the same fractional-order β and high voltage crosslinking confidence h_{e_1}. As a result, the ω_1 and $\bar{\omega}_1$ membrane amperage parameters have a significant causal relationship with CS.

Results and discussion

Implementations in the modern environment can benefit mostly from fractional-order complexities. It may result in interlinkages, such as transitions between different reliability levels, intermittent behaviour and chaos behaviour. These extremely complicated characteristics are demonstrated by the nonlinear, fractional-order neurobiological framework we formed. A deeper examination of the fractional-order excitatory mechanisms may benefit from the fascinating neurological reactions revealed by the hypothetical computation and computational consequences. This study contains a corresponding fractional-order derivative to implement the features of a fast–slow FHR framework. This has been investigated to see how fractional expressions affect the system's complexities and distinguish this system through the integer-order FHR framework, which displays elliptic spurting. It displays various oscillatory forms and spike intensities depending on different kinds of settings. It displays various oscillatory sorts and spike frequency distributions depending on different kinds of settings. The fractional exponent significantly contributes to the creation and destruction of explosions. The framework's capacity is altered as a result. It also helps us comprehend how interacting mechanisms interpret data. Chaos and fractional-order excitatory mechanisms can

be synchronized, and this has the potential to be applied to restrict protected communication. We discovered that signals generated limited fractional orders in the both scenarios biological neurotransmitter. The switchover regions for different fractional orders with different criteria, such as the dormant states, are addressed. The importance of our task resides in the fact that we demonstrate the CS set of criteria in fractionally synchronous machines while taking into account neurologically pertinent electronic power correlations, i.e., reversible merging for two nerve cells exhibiting a wide variety of perturbations. For a reversible or discrepancy configuration coupling strategy, it can be expanded to a system of neural connections with these kinds of fractional-order neurotransmitters.

Conclusion

In this research, we introduced a novel discrete fractional FitzHugh–Rinzel neuron model that concentrates on both commensurate and incommensurate orders. The analysis indicates that the nonlinear dynamic profiles are varied and pragmatically rich. By computing the modelling phase depictions and bifurcation illustrations and predicting the tendencies of the proposed fractional FitzHugh–Rinzel for commensurate and incommensurate orders, the interactions of the proposed

framework were addressed. The findings demonstrate that fractional FitzHugh–Rinzel discrete systems generate a dynamic response with both a significantly higher level of creativity and a wider variety of chaos domains when the incommensurate orders are diversified. In order to regulate and synchronize the proposed framework, efficient regulatory restrictions that force the regions to asymptotically congregate towards zero were finally proposed. Our findings were verified by employing MATLAB-based simulation studies. It is becoming difficult to find a neuron framework with appropriate configurations that exhibits different interactive effects while incorporating the fractional-order constituent into the mechanism. This kind of research into excitatory neurobiological mechanisms is constrained by the diversity of computationally intensive problems that can be solved, but certain strategies for analysing fractional-order complexities have previously been developed. Recognizing the complexities of signals and systems, interference of electrical impulses, neuronal mechanisms in neurotransmitter systems, various neurocomputational functionalities and characteristics of various sorts of machine learning algorithms and connectivity for highly complicated neurodevelopment in both healthy and malignant states, such as neurodegenerative diseases, may be considerable.

Declaration of competing interest

The authors declare that they have no known competing financial interests or personal relationships that could have appeared to influence the work reported in this paper.

Data availability

No data was used for the research described in the article

Acknowledgements

References

[1] Alexander GD, Aurel AL, Jonethan DV. Information theory in neuroscience. J Comput Neurosci 2011;30:1–5.

[2] Yao SW, Mabrouk SM, Inc M, Rashed AS. Analysis of double-chain deoxyribonucleic acid dynamical system in pandemic confrontation. Results Phys 2022;42:105966.

[3] Inc M, Khan MN, Ahmad I, Yao SW, Ahmad H, Thounthong P. Analyzing time-fractional exotic options via efficient local meshless method. Results Phys 2020;19:103385.

[4] Yao SW, Faridi WA, Asjad MI, Jhangeer A, Inc M. A mathematical modelling of a atherosclerosis intimation with Atangana-Baleanu fractional derivative in terms of memory function. Results Phys 2021;27:104425.

[5] Dehingia K, Yao SW, Sadri K, Das A, Sarmah HK, Zeb A, Inc M. A study on cancer-obesity-treatment model with quadratic optimal control approach for better outcomes. Results Phys 2022;42:105963.

[6] Zafar ZUA, Hussain MT, Inc M, Baleanu D, Almohsen B, Oke AS, Javeed S. Fractional-order dynamics of human papillomavirus. Results Phys 2022;34:105281.

[7] Rinzel J. Bursting oscillation in an excitable memberane model. In: Ordinary and partial differential equations proceedings of the eighth dundee conference. Berlin: Springer-Verlag; 1985, p. 304–16.

[8] Sherman A, Rinzel J. Rhythmogenic effects of weak electronic coupling in neuronal model. Proc Natl Acad Sci 1992;89:2471–4.

[9] Bertram R, Butte MJ, Kiemei T, Sherman A. Topological and phenomeno-logical classification of bursting oscillations. Bull Math Biol 1995;57:413–39.

[10] Holden L, Erneux T. Slow passage through a hopf bifurcation: form oscillatory to steady state solutions. SIAM J Appl Math 1993;53:1045–58.

[11] Smolen P, Terman D, Rinzel J. Properties of a bursting model with two slow inhibitory variables. SIAM J Appl Math 1993;53:861–91.

[12] de Vries G. Multiple bifurcations in a polynomial model of bursting oscillations. J Nonlinear Sci 1998;8:281–316.

[13] Rush ME, Rinzel J. Analysis of bursting in thalamic neuron model. Biol Cybernet 1994;71:281–91.

[14] Izhikevich EM. Neural excitability, spiking and bursting. Int J Bifur Chaos 2000;10:1171–266.

[15] Lundstrom BN, Famulare M, Sorensen LB, Spain WJ, Fairhall AL. Sensitivity of firing rate to input fluctuations depends on time scale separation between fast and slow variables in single neurons. J Comput Neurosci 2009;27:277–90.

[16] Tai CF, Roppolo JR, de Grost WC. Analysis of nerve conduction block induced by direct current. J Comput Neurosci 2009;29:201–10.

[17] Westerlund S, Ekstam L. Capacitor theory. IEEE Trans Dielectr Electr Insul 1994;1:26–39.

[18] Magin RL. Fractional calculus in bioengineering. Crit Rev Biomed Eng 2004;32:1–104.

[19] Magin RL. Fractional calculus models of complex dynamics in biological tissues. Comput Math Appl 2010;59:1586–93.

[20] Magin RL, Ovadia M. Modeling the cardiac tissue electrode interface using fractional calculus. J Vib Control 2008;14:1431–42.

[21] Lundstrom BN, Higgs MH, Spain WJ, Fairhall AL. Fractional differentiation by neocortical pyramidal neurons. Nat Neurosci 2008;11:1335–42.

[22] Atangana A, Goufo EFD. The Caputo–Fabrizio fractional derivative applied to a singular perturbation problem. Int J Math Model Numer Optim 2019;9:241–53.

[23] Atangana A, Koca I. Model of thin viscous fluid sheet flow within the scope of fractional calculus: Fractional derivative with and no singular kernel. Fund Inform 2017;151(1–4):145–59.

[24] Atangana A. On the new fractional derivative and application to nonlinear Fisher's reaction–diffusion equation. Appl Math Comput 2016;273:948–56.

[25] Atangana A, Alkahtani BST. Modeling the spread of rubella disease using the concept of with local derivative with fractional parameter : Beta-derivative. Complex 2016;21:442–51.

[26] Atangana A. On the stability and convergence of the time-fractional variable order telegraph equation. J Comput Phys 2015;293:104–14.

[27] Anastosio TJ. The fractional-order dynamics of brainstem vestibulo-oculomotor neurons. Biol Cybern 1994;72:69–79.

[28] Fusi S, Drew PJ, Abbott LF. Cascade models of synaptically stored memories. Neuron 2005;45:599–611.

[29] Li CP, Zhang FR. A survey on the stability of fractional differential equations. Eur Phys J-Special Top 2011;193:27–47.

[30] Margarita R, Sergei R, José TM, Trujillo JJ. Stability of fractional order systems. Math Probl Eng 2013;2013.

[31] Matignon D. Stability results for fractional differential equations with applications to control processing. 1996, p. 963–8.

[32] Jocelyn S, Christophe F. On stability of commensurate fractional order systems. Int J Bifur Chaos 2012;22:1250084.

[33] Changpin L, Yutian M. Fractional dynamical system and its linearization theorem. Nonlinear Dyn 2013;71:621–33.

[34] Zhiliang W, Dongsheng Y, Huaguang Z. Stability analysis on a class of nonlinear fractional-order systems. Nonlinear Dyn 2016;86:1023–33.

[35] Ivo P. Stability of fractional-order systems with rational orders. 2008, arXiv preprint arXiv:0811.4102.

[36] Bohdan D, Yuri L. Complex oscillations and limit cycles in autonomous two-component incommensurate fractional dynamical systems. Math Balkanica 2012;26:65–78.

[37] Gomaa RA, Ahmed SE, Ahmed MS. Fractional-order sinusoidal oscillators: design procedure and practical examples. IEEE Trans Circuits Syst I Regul Pap 2008;55:2051–63.

[38] Ansar Trächtler. On BIBO stability of systems with irrational transfer function. 2016, arXiv preprint arXiv:1603.01059.

[39] Rinzel J, Troy WC. Bursting phenomena in a simplifed oregonator fow system model. J Chem Phys 1982;76:1775–89.

[40] Honorkamp J, Mutschler G, Seitz R. Coupling of a slow and a fast oscillator can generate bursting. Bull Math Biol 1985;47:1–21.

[41] Rinzel J. A formal classifcation of bursting mechanisms in excitable systems, in mathematical topics in population biology, morphogenesis and neurosciences. Lecture Notes in Biomathematics, vol. 71, Berlin: Springer-Verlag; 1987, p. 267–81.

[42] Izhikevich EM. Synchronization of elliptic bursters. SIAM Rev 2001;43:315–44.

[43] Izhikevich EM. Neural excitability, spiking and bursting. Int J Bifurcation Chaos 2000;10:1171–266.

[44] Izhikevich EM. Simple model of spiking neurons. IEEE Trans Neural Netw 2003;14:1569–72.

[45] FitzHugh R. Impulses and physiological states in theoretical models of nerve membrane. Biophys J 1961;1:445–66.

[46] FitzHugh R. Mathematical models of excitation and propagation in nerve. New York: McGraw- Hill; 1969,

[47] Weinberg SH. Membrane capacitive memory alters spiking in neurons described by the fractional-order Hodgkin–Huxley model. PLoS One 2015;10:e0126629.

[48] Teka WW, Upadhyay RK, Mondal A. Spiking and bursting patterns of fractional-order Izhikevich model. Commun Nonlinear Sci Numer Simul 2018;56:161–76.

[49] Shi M, Wang Z. Abundant bursting patterns of a fractional-order Morris-Lecar neuron model. Commun Nonlinear Sci Numer Simul 2014;19:1956–69.

[50] Wojcik J, Shilnikov A. Voltage interval mappings for an elliptic bursting model. In: Gonzlez-Aguilar H, Ugalde E, editors. Nonlinear dynamics new directions, Vol. 12. Cham: Springer; 2015, p. 195–213.

[51] Abdeljawad T. On Riemann and Caputo fractional differences. Comput Math Appl 2011;62:1602–11.

[52] Atici FM, Eloe P. Discrete fractional calculus with the nabla operator. Electron J Qual Theory Differ Equ 2009;3:1–12.

[53] Wu GC, Baleanu D. Discrete fractional logistic map and its chaos. Nonlinear Dynam 2014;75:283–7.

[54] Li C, Chen Y, Kurths J. Fractional calculus and its applications. Philos Trans R Soc A. 2013;371:20130037.

[55] Rosenblum MG, Pikovsky AS, Kurths J. From phase to lag synchronization in coupled chaotic oscillators. Phys Rev Lett 1997;78:4193.